Unique growth and morphology properties of Clade 5 *Clostridioides difficile* strains revealed by single-cell time-lapse microscopy

John W. Ribis[1,2], César A. Nieto-Acuña[3], Qiwen Dong[1], Nicholas V. DiBenedetto[1,2], Anchal Mehra,[4] Irene Nagawa,[1] Imane El Meouche,[5] Bree B. Aldridge,[1] Mary J. Dunlop,[6] Rita Tamayo,[4] Abyudhai Singh,[3] Aimee Shen[1*]

Affiliations

[1]Department of Molecular Biology and Microbiology, Tufts University School of Medicine, Boston, Massachusetts, USA, [2] Graduate School of Biomedical Sciences, Tufts University School of Medicine, Boston, Massachusetts, USA. [3]Department of Electrical and Computer Engineering, University of Delaware, Newark, DE 19716, USA. [4]Department of Microbiology and Immunology, University of North Carolina at Chapel Hill School of Medicine, Chapel Hill, NC, USA, [5]INSERM, Université de Paris Cité, Université Sorbonne Paris, Nord, IAME, F-75018, Paris, France, [6]Biomedical Engineering, Boston University, Boston, MA 02215.

[*]Address correspondence to
Aimee Shen, aimee.shen@tufts.edu
Phone number: (617)636-3792

Abstract

Clostridioides difficile is a major One Health threat as an important gastrointestinal pathogen of both humans and agricultural animals. The *C. difficile* species can be subdivided into 5 main clades, with Clade 5 currently undergoing speciation from Clades 1-4. Since Clade 5 strains are found more frequently in agricultural animals and can cause zoonotic infections, Clade 5 strains likely have evolved phenotypes that distinguish them from Clade 1-4 strains. Here, we compare the growth properties of Clade 5 strains to Clade 1, 2, and 4 strains using an anaerobic time-lapse microscopy system coupled with automated image analysis. These analyses revealed that Clade 5 strains grow faster than Clade 1, 2, and 4 strains and are more likely to form long chains of cells. Notably, the chaining phenotype was not shared among all Clade 5 strains examined, since 1 of the 9 strains did not form chains. Genomic analyses of the Clade 5 strains revealed that the orientation of the *cmr* switch, an invertible DNA element controlling the expression of a signal transduction system that regulates chaining, correlates with the propensity of a given Clade 5 strain to form chains. Taken together, Clade 5 strains appear to have distinct growth properties that allow them to inhabit more diverse ecological niches.

43 **Introduction**

44

45 *Clostridioides difficile* is a leading cause of nosocomial infection in the United
46 States, with approximately 500,000 new infections and 14,000 deaths attributed to this
47 organism annually (1, 2). As an obligate anaerobe, *C. difficile* relies on its ability to form hardy,
48 metabolically dormant spores to survive outside the gut environment and transmit disease (3).
49 When *C. difficile* spores are ingested by susceptible hosts (4, 5), they encounter bile salt signals
50 in the small intestine that trigger their germination. These stimuli allow them to exit dormancy
51 and outgrow into vegetative cells, which colonize the colon and secrete toxins that damage gut
52 epithelial tissue (6). This damage triggers a significant inflammatory response that can cause
53 disease pathologies ranging from mild diarrhea to pseudomembranous colitis, and even death
54 (2, 4). Beyond these acute complications, *C. difficile* frequently causes recurrent infections
55 (~20% of infections), which can lead to more severe disease symptoms (14–16) (2, 7, 8).
56 Notably, as a species, *C. difficile* exhibits tremendous genetic diversity (9-11). Genomic
57 analyses indicate that *C. difficile*'s core genome represents only ~10-20% of its pan-genome (9,
58 10). The extreme plasticity of the "open" pan-genome of *C. difficile* likely helps the bacterium
59 inhabit the gastrointestinal tract of diverse animals, from mammals to invertebrates, and
60 environmental reservoirs like sewage and compost (12). Multi-locus sequence typing (MLST)
61 analyses have revealed that the *C. difficile* species comprises 5 distinct phylogenetic clades that
62 can be further subdivided into different ribotypes (RTs) or sequence types (STs) (10, 13). While
63 whole-genome sequencing analyses identified three additional cryptic clades, subsequent
64 analyses have revealed that the genomic divergence between the 5 main clades and three
65 additional cryptic clades is so significant that the cryptic clade species fall below the threshold
66 determined by average nucleotide identity (ANI) to qualify as part of the *C. difficile* species (10,
67 14).
68 Between the five remaining phylogenetic clades, there are notable differences in
69 geographic and host distributions. Clade 1 is the largest and most heterogeneous (and likely
70 ancient) clade, containing over 200 STs that have the broadest geographic distribution (15, 16).
71 It includes both toxin-producing and non-toxigenic strains, including the well-characterized,
72 genetically tractable toxigenic strain 630 (9). Clade 2 harbors epidemic-associated strains found
73 within the ribotype 027 (RT027) lineage. Strains from this ribotype have been associated with

74 outbreaks in hospitals, particularly in North America, due to their frequent resistance to
75 fluoroquinolones (17-19). These epidemic strains can also cause severe disease symptoms in
76 part due to their production of three toxins: TcdA, TcdB, and CDT (binary toxin) (6). Although
77 RT027 strains have frequently been associated with "hypervirulence," there is considerable
78 phenotypic diversity within this lineage with respect to virulence, toxin production levels, and
79 sporulation (20-22).
80 Clade 3 strains are relatively uncommon and harbor a unique cell surface due to their
81 lack of CwpV production (23), but phenotypic analyses of biofilm formation and motility
82 suggest that they share similarities with Clade 2 strains like R20291 (24). Clade 4 contains
83 RT017 (ST37) strains that only encode a single toxin, TcdB (i.e., TcdA–CDT–), and are often
84 clindamycin- and fluoroquinolone-resistant. RT017 strains have been associated with outbreaks
85 in Europe and North America and are the most common strains found in Asia (25). Clade 5 is
86 the most genetically distant from the other 4 main *C. difficile* clades (94) and is thought to have
87 emerged before Clades 1-4 (26). While the ANI for Clades 1-4 ranges between 97.1 - 99.8%,
88 Clade 5 strains exhibit ANI values around 96%, which is close to the ANI value demarcation
89 used by NCBI to define organisms of the same species (10, 14). Thus, Clade 5 strains appear to
90 be actively diverging from Clades 1-4 (10).
91 Clade 5 strains are an increasing problem in healthcare and agricultural settings because
92 they can cause severe disease in humans and are commonly found in livestock, particularly pigs
93 (12, 27). While other *C. difficile* strains have been known to infect both humans and animals,
94 only Clade 5 strains have been associated with zoonotic transmission from both animal-to-
95 human and human-to-animal. The mechanisms underlying this bidirectional zoonotic
96 transmission are poorly understood, but the increased carriage of antimicrobial resistance genes
97 by Clade 5 strains may contribute to their ability to persist in livestock and humans. The
98 prevalence of antibiotic resistance genes in Clade 5 strains has major implications for One
99 Health, particularly with respect to antibiotic use in agriculture and humans (12, 27, 28).
100 Furthermore, Clade 5 strains frequently cause community-acquired infections, which likely
101 reflects wide environmental distribution and highlights the importance of understanding the
102 unique properties of this group of strains. Indeed, a recent genomic analysis suggests that
103 RT078/ST11 strains within Clade 5 frequently carry zinc acquisition and homeostasis genes
104 (11).

105 Despite numerous genomic analyses revealing the remarkable genetic diversity of *C.*
106 *difficile* strains, relatively few studies have investigated the phenotypic diversity between strains
107 from different clades. Clade-specific differences in colony morphology between Clade 5 strains
108 relative to Clade 1-4 strains have been described in a limited set of analyses (26, 29), suggesting
109 that differences in growth and/or cellular morphology may exist within clades. While
110 differences in bulk growth rates between *C. difficile* strains have been reported (30), most
111 phenotypic analyses have been conducted on a limited subset of strains within a given clade.
112 Indeed, no systematic comparisons of the growth properties of the different clades or
113 comparisons of cell morphology have been performed to date.
114 Here, we compare the growth properties of multiple strains derived from the four
115 predominant main phylogenetic clades of *C. difficile* (Clade 1, 2, 4, and 5) using anaerobic
116 time-lapse microscopy. These analyses unexpectedly revealed striking differences in the growth
117 and cell morphology of the Clade 5 lineage relative to strains from Clades 1, 2, and 4. These
118 morphological differences correlate with the orientation of the *cmr* switch, which has previously
119 been implicated in modulating cell and colony morphology and cell chaining (31). Thus, the
120 *cmr* switch appears to be an important contributor to the chaining phenotype frequently
121 observed in Clade 5 strains.
122
123 **Results**
124
125 **Development of a simple method for time-lapse imaging under anaerobic conditions**
126
127 Time-lapse imaging of single cells has been widely used in bacteria due to the growing
128 appreciation that clonal bacterial populations can exhibit considerable phenotypic heterogeneity,
129 with implications for antibiotic resistance and virulence (31-35). However, live single-cell
130 analyses in *C. difficile* have been complicated by its inability to grow in the presence of
131 atmospheric oxygen (36). While there have been limited reports of live cell time-lapse
132 microscopy of *C. difficile*, these analyses have required custom growth chambers to maintain
133 anaerobic conditions (37), which may limit the accessibility of these experimental systems to
134 most investigators.

135 To overcome these limitations, we established a simple system that relies solely upon
136 commercially available reagents and materials to grow *C. difficile* cells under anaerobic
137 conditions. This system uses gas-tight, adhesive Gene Frames™, which have been used
138 extensively in imaging applications for bacteria (38). Notably, the gas-impermeability of these
139 commercial seals allows maintenance of anaerobic conditions when the agarose pads, which
140 contain growth media, are prepared in the anaerobic chamber (**Figure 1**).
141

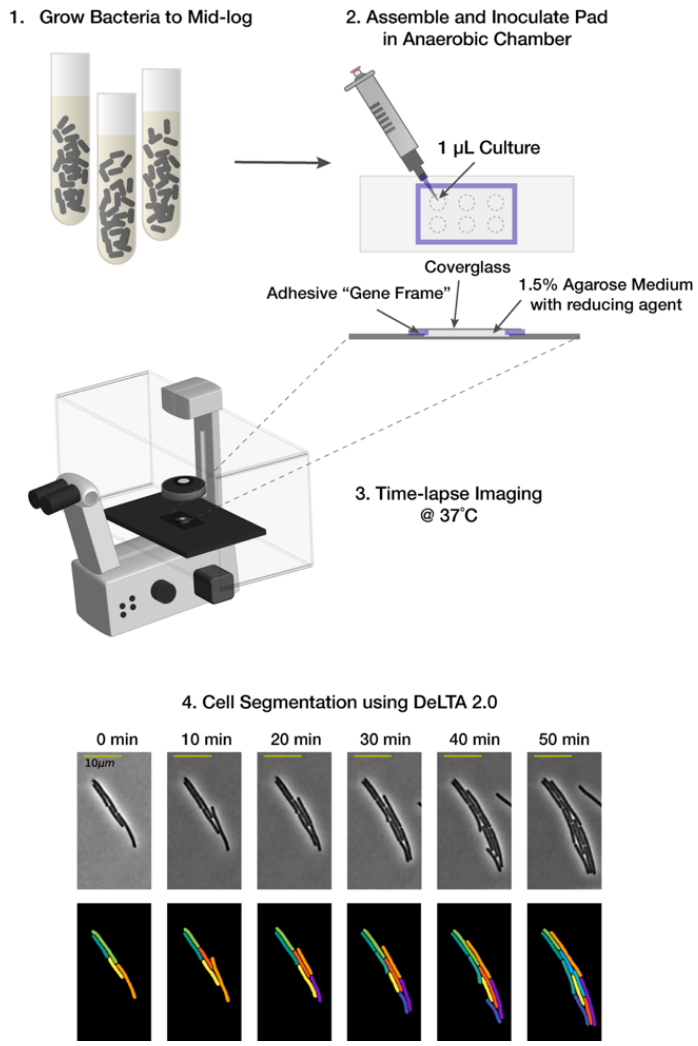

142
143
144 **Figure 1. Schematic of the anaerobic single-cell imaging set-up**. Exponentially growing *C. difficile*
145 cells in TY medium supplemented with cysteine (TYC) are spotted onto a 1.5% agarose pads formed
146 within gas-tight adhesive Gene Frames inside the anaerobic chamber. Up to 6 strains can be spotted
147 onto a pad. The pad is sealed with a coverslip, and the imaging chamber is removed from the anaerobic
148 chamber and transferred to a heated (37˚C) microscope stage. Time-lapse microscopy is used to
149 visualize the growth of individual bacterial cells for 2-6 hrs. The output data is segmented and tracked
150 with the DeLTA 2.0 Python package (191). An example filmstrip of strain 630 grown on TYC medium
151 over time (Bottom).

152 Gene Frames also allow highly uniform, thick agarose pads to be generated, which are properties
153 critical for conducting automated time-lapse microscopy analyses and enabling *C. difficile* to
154 grow in a sealed system under ambient conditions.
155
156 **Time-lapse microscopy reveals clade-specific differences in elongation rate and cell length**
157
158 Following the establishment of our time-lapse imaging setup, we compared the single-
159 cell growth properties of representative *C. difficile* strains from Clade 1 (630, ribotype (RT)
160 012), Clade 2 (R20291, RT027), Clade 4 (M68, RT017), and Clade 5 (M120, RT078) (**Figure**
161 **2, Table 1**). We did not have access to Clade 3 strains, so these were not included in this study.
162 The four "representative" strains were all isolated from patients with *C. difficile*-associated
163 disease and are frequently used as reference genomes for their clades and ribotype groups.
164 Notably, RT027 (ST1), RT017 (ST45), and RT078 (ST11) strains are from ribotypes/
165 multilocus sequencing types that are frequently isolated from patients with *C. difficile* infection
166 (CDI) (12, 19, 22, 25).
167 To quantify the growth properties of single cells visualized by time-lapse microscopy,
168 we used DeLTA 2.0, a Deep Learning for Time-lapse Analysis (DeLTA) software that allows
169 rapid and accurate segmentation and tracking of bacteria growing in two dimensions on agarose
170 pads (39, 40). This software uses deep convolutional neural networks to obtain information on
171 the growth properties of individual cells growing in microcolonies on agarose pads. The
172 segmentation and tracking of *C. difficile* cells was highly accurate (**Figure 1**), and minimal user
173 input or post-image processing was needed to obtain growth property measurements.
174 Robust growth was observed for all strains using our system, with Clade 5 strain M120
175 elongating the fastest (2.1 doublings/hr), followed by Clade 2 strain R20291 (1.8 doublings/hr),
176 and then Clade 1 strain 630 and Clade 4 strain M68 (1.6-1.7 doublings/hr) (**Fig 2A**). This
177 elongation rate was defined as doublings/hr to indicate the number of times that a cell's size
178 doubles in one hour. For example, an elongation rate of 2 doublings/hr means that the cell size
179 doubled twice in 1 hr, which corresponds to an exponent of 2ln(2) 1/hr. Notably, the elongation
180 rate (doublings/hr) should not be confused with doubling time, or generation time, which are
181 defined as the length of *time* that it takes before a bacterium divides. Instead, the elongation rate
182 reflects how fast the cell is increasing in length over time. Nevertheless, elongation rate and

183 doubling time are related because most cells undergo a division event when they reach twice
184 their original size.

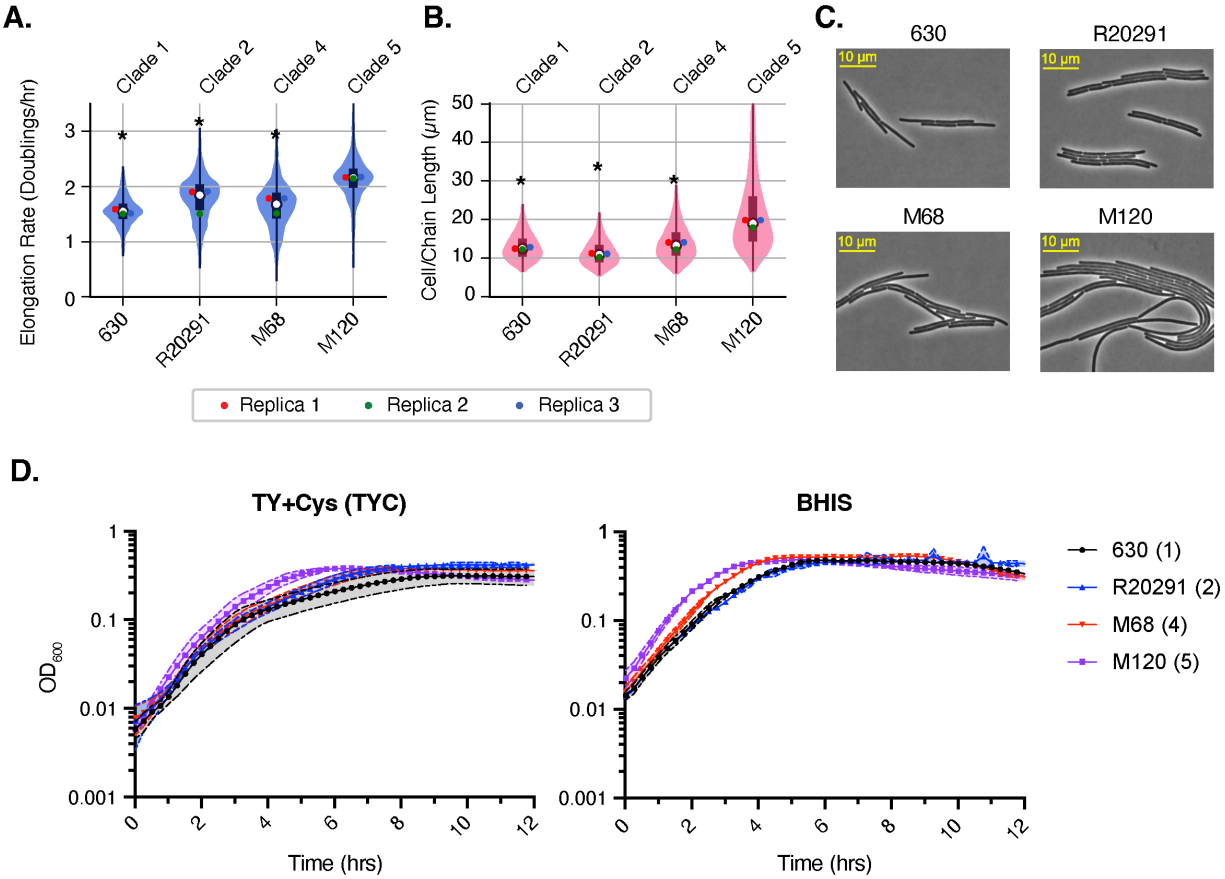

185
186
187 **Figure 2. Clade 5 strain M120 elongates more quickly and exhibits cell chaining.** A. Violin plot of
188 the elongation rates measured during time-lapse microscopy analyses of strains 630 (Clade 1), R20291
189 (Clade 2), M68 (Clade 4), M120 (Clade 5) grown on TY supplemented with cysteine (TYC) agar. Data
190 are from three biological replicates, with the mean of each replicate shown as a point on the violin. B.
191 Violin plot of the cell length measured during time-lapse microscopy for strains 630 (Clade 1), R20291
192 (Clade 2), M68 (Clade 4), M120 (Clade 5). Each replicate mean is shown as a point on the violin.
193 Statistical significance for A and B was determined by comparing the mean of the three replicates of
194 Clade 1, 2, and 4 strains to the Clade 5 M120 strain using a Kruskal-Wallis test * $p < 0.05$. C. Phase-
195 contrast image from time-lapse microscopy movies. Scale bar is 10 μm. D. Optical density-based
196 analyses of bulk population growth of the indicated strains in TYC or BHIS medium. The number in
197 brackets indicates the clade to which a given strain belongs.
198

199 Importantly, the differences in single-cell elongation rates measured for the four strains
200 using DeLTA were also observed in bulk population analyses of their growth using optical
201 density in TYC and BHIS media (**Figure 2D**). These analyses confirmed that the Clade 5 strain
202 M120 grows faster (using optical density as a proxy for bacterial growth) than the Clade 1, 2,

203 and 4 strains analyzed. In contrast, negligible differences in bulk growth rates for Clade 1, 2,
204 and 4 strains were observed (**Figure 2A**), consistent with the relatively subtle difference
205 observed in the single-cell elongation rates measured for the Clade 2 R20291 strain relative to
206 the Clades 1 and 4 strains.
207 The Clade 5 strain M120 exhibited another distinct growth property from the strains
208 from Clades 1, 2, and 4. While strains from Clades 1, 2, and 4 produced cells of similar length
209 prior to division, with an average cell size of ~13 µm prior to division, cells of Clade 5 strain
210 M120 were significantly longer, appearing as long filaments (or chains) with an average length
211 of 22 µm but chains close to 50 µm readily being measured (**Figure 2B**). These filaments or
212 chains also appeared to bend readily (**Figure 2C**). Notably, to visualize an entire filament (or
213 chain), it was necessary to stitch together several fields of view, revealing that the bacterial
214 filaments (or chains) approached several hundred microns and even up to ~1 mm in length
215 (**Figure 3**). To determine whether strain M120 forms filaments, i.e. long cells that lack division
216 septa, or chains of cells, i.e. cells that remain attached despite forming division septa, we
217 incorporated the lipophilic fluorescent dye FM4-64 which visualizes membranes (Pogliano
218 1999), directly into the agarose pads. This stain revealed division septa throughout the length of
219 the cell, indicating that the extremely long cells were not filaments but instead extended chains
220 of cells (**Figure 3, inset**). Since the spacing between division septa generated cells that were
221 relatively similar in length to the other *C. difficile* strains analyzed, Clade 5 strain M120 is
222 distinguished by a decreased efficiency in cell separation.
223

224 **Clade 5 clinical isolates typically form long chains and grow more quickly than strains**
225 **from other clades**
226

227 Since prior work indicated that Clade 5 strains produce colony morphologies distinct from
228 Clade 1, 2, and 4 strains (26), we sought to determine whether the (i) striking cell chaining
229 phenotype and (ii) faster growth rate observed in Clade 5 strain M120 is observed in other
230 Clade 5 strains. To address these questions, we compared the single-cell growth properties on
231 TYC agarose of 5 additional Clade 5 clinical isolates obtained from three separate hospitals
232 (**Table 1**) using time-lapse microscopy analyses (**Figure 2**). Clade 1 strain 630 was included as
233 a control since it does not form chains under these conditions.

234

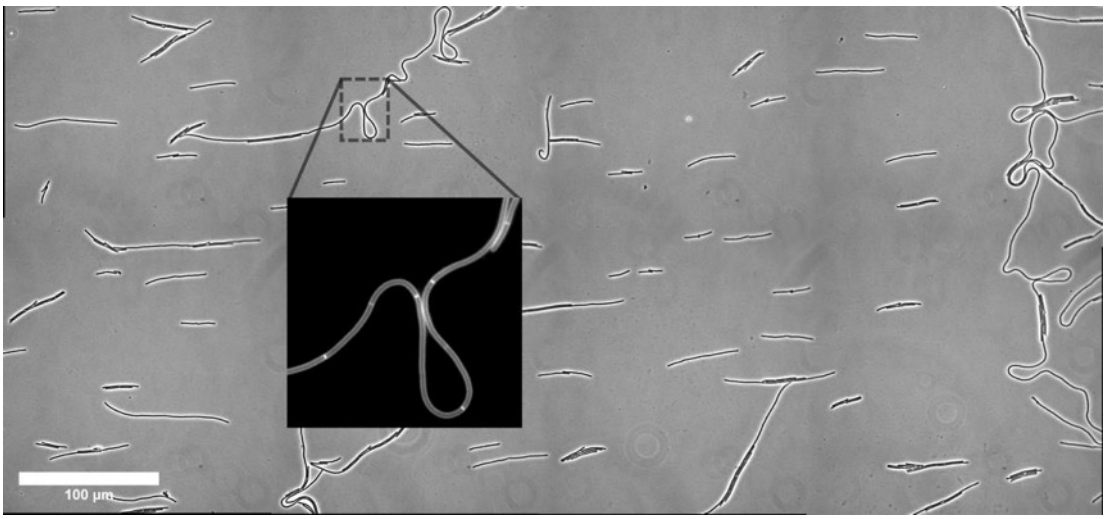

235
236
237 **Figure 3. *C. difficile* Clade 5 can form large heterogenous chains.** Large mosaic phase-contrast
238 image of the Clade 5 *C. difficile* strain M120. Zoomed image shows chains revealed by staining with
239 the membrane dye FM4-64. Image was stitched from 8 individual fields of view at 63x magnification.
240 Scale bar is 100 µm.
241

242 These analyses revealed that all but one of the Clade 5 strains tested formed long chains,
243 with TAL29600 forming the longest chains (29 µm on average, **Figure 4A-C**). In contrast,
244 strain TAL29996 formed shorter chains that were comparable in length to those observed for
245 strains from Clades 1, 2, and 4 (12-13 µm, **Figures 2B, 4C**). Notably, DeLTA over-estimated
246 cell length in Clade 5 strains that form chains because it could not identify cells that had formed
247 division septa (based on FM4-64 staining) but had not yet initiated cell separation.
248 To overcome this limitation and accurately quantify cell length within long chains, namely the
249 distance between division septa, we modified our image processing pipeline to use a
250 thresholding method to detect division septa. After generating masks in DeLTA to segment the
251 chains, we modified the mask so that only the interior of the contour was analyzed. We then
252 applied an adaptive thresholding method to identify division septa based on their elevated long
253 chains do not produce cells that are dramatically longer than strains that do not form chains;
254 cells within the Clade 5 strains that produced the longest chains had average cell lengths
255 (TAL29600 and TAL30550, 14 and 12 µm, respectively) that were 30-50% longer than strains
256 that do not form chains like strains 630 (Clade 1, 8.5 µm) and TAL29996 (Clade 5, 9.4 µm).
257 Notably, even though TAL29996 did not form long chains like the other Clade 5 strains
258 analyzed, it elongated at rates similar to those of other Clade 5 strains (2.1 doublings/hr vs. 1.7

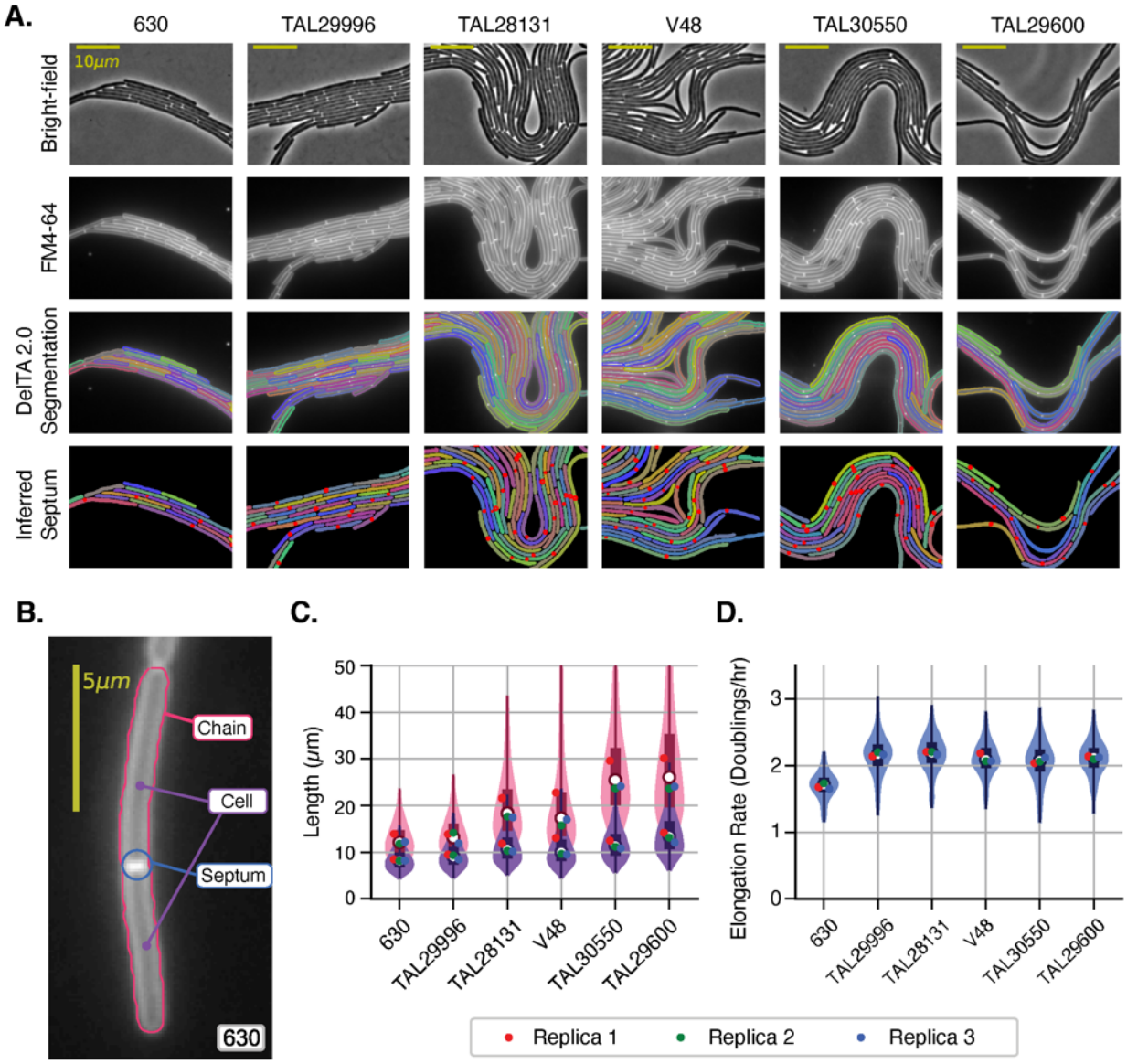

Figure 4. Faster growth is a common feature of Clade 5 strains, but the chaining phenotype is not fully penetrant in Clade 5 strains. (A) Phase-contrast microscopy images from time-lapse microscopy studies of Clade 5 strains; Clade 1 strain 630 is included for comparison. Fluorescence microscopy was used to visualize the FM4-64 stain incorporated into the agarose pads. Masks generated using DeLTA 2.0 are shown, with the bottom panel showing division septa identified with our adaptive thresholding approach. (B) Example image showing the parameters identified using DeLTA 2.0 combined with our adaptive threshold method for detecting division septa within a chain of cells. (C) Cell length measured based on automated DeLTA 2.0 analyses (pink violin plot) or DeLTA 2.0 combined with adaptive threshold analyses (purple violin plot). The former method is more likely to measure chain length, while the latter method more accurately measures cell length. (D) Violin plot of the elongation rates measured for the indicated strains based on three biological replicates. For all the violin plots shown, each replicate mean is shown as a point on the violin, and statistical significance was determined by comparing the mean of the three replicates using a Kruskal-Wallis test * $p < 0.05$.

276 doublings/hr for Clade 1 strain 630**, Figure 4D**). Taken together, these analyses strongly
277 suggest that Clade 5 strains grow faster than Clade 1, 2, and 4 strains and are more likely to
278 form chains presumably because their cell separation mechanisms are less efficient.
279 While the long chains formed by Clade 5 strains limited the number of divisions that
280 could be analyzed within a given field using time-lapse microscopy, the faster elongation rates
281 measured on the agarose pads were also observed in bulk analyses of growth in broth culture.
282 These optical density-based analyses revealed that Clade 5 strains all grow faster than Clade 1,
283 2, and 4 strains irrespective of their ability to form chains or the growth media used (**Figure**
284 **S1**).
285 To assess whether these conclusions could be generalized to additional Clade 5 strains
286 vs. Clade 1, 2, and 4 strains, we analyzed the growth of additional strains from all four clades in
287 broth culture. These analyses confirmed that Clade 1, 2, and 4 strains grow at similar rates,
288 which are slower than those measured for the nine Clade 5 strains analyzed in both TYC and
289 BHIS media (**Figure S1**).
290
291 **Cell chaining in Clade 5 strains is not dependent on growth on a solid medium.**
292
293 *C. difficile* has previously been shown to promote cell elongation and chain formation
294 upon induction of the *cmrRST* locus (31), which encodes a signal transduction system.
295 Expression of this locus is also responsive to c-di-GMP levels (29), which increases in cells
296 grown on solid surfaces such as in a biofilm or on an agar plate (29). To determine whether the
297 chaining phenotype observed in most Clade 5 strains is induced by growth on a surface, we
298 assessed whether cell chaining would be observed in cells grown in broth culture. The Clade 5
299 strains along with strains from other clades were grown to log-phase in rich media, and their
300 ability to form chains was assessed by visualizing division septa with the fluorescent D-amino
301 acid label, HADA. Chains of cells were still observed in the Clade 5 strains by time-lapse
302 microscopy analyses, although the chains formed in broth culture were not as long as those
303
304 observed during growth on the agarose pads (**Figure 5, S2**). Chains were also observed in 4
305 additional Clade 5 strains analyzed during exponential-phase growth in broth culture.
306 Interestingly, two of the Clade 5 strains, V48 and WU66, did not appear to incorporate the

307 HADA label efficiently, and the cells appeared lighter in phase-contrast images despite
308 undergoing the fixation process shortly after HADA addition. It is unclear why the HADA was
309 poorly incorporated by these strains across multiple independent experiments. Regardless, these
310 results indicate that many Clade 5 strains undergo cell separation less efficiently than strains
311 from other clades irrespective of whether they are grown on a solid surface or in broth culture.
312

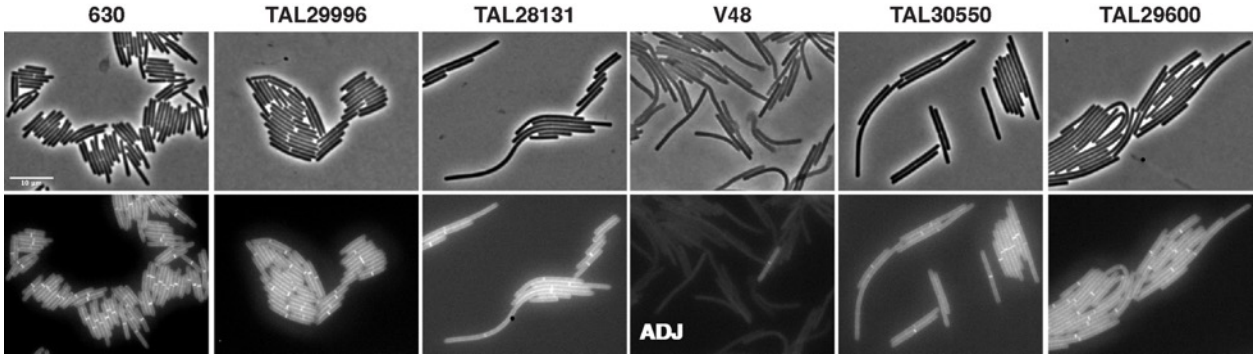

313
314 **Figure 5. Clade 5 strains form chains during logarithmic growth in broth culture**. Representative
315 micrographs showing phase-contrast (top) and peptidoglycan labeling with the fluorescent D-amino
316 acid, HADA, (bottom) following growth in rich broth (BHIS) to logarithmic phase. Scale bar, 10 µm.
317 Data are representative of multiple independent experiments. **ADJ** indicates that the brightness of the
318 image was enhanced to detect HADA labeling in V48.
319
320
321 **Cell length does not correlate with the propensity to sporulate.**
322
323 We next wondered whether the propensity to form chains impacts the ability of Clade 5
324 strains to sporulate because analyses in *Bacillus subtilis* suggest that smaller cells, such as those
325 formed during stationary phase growth (41), may concentrate proteins involved in the
326 phosphorelay that induces sporulation. In *B. subtilis*, the decrease in cell length helps the kinase
327 KinA reach the threshold concentration needed to trigger sporulation initiation (42, 43).
328 Although *C. difficile* lacks homologs of KinA and other components of the phosphorelay
329 system, it is possible that the longer cell length observed in Clade 5 strains may similarly reduce
330 their ability to induce sporulation by diluting the levels of a currently unknown sporulation
331 regulator. To test this hypothesis, we analyzed the propensity of Clade 5 strains to form spores
332 when plated on 70:30 sporulation medium using phase-contrast microscopy and heat resistance
333 assays.
334 Striking differences in the frequency of spore formation were observed across the Clade
335 5 strains, with several strains exhibiting close to 100% sporulation levels (**Figure 6A, S3**).

336 Although TAL29600, which forms the longest chains of the strains tested, exhibited extremely
337 low levels of sporulation (0.003%), we did not observe a correlation between sporulation and
338 cell length among the strains (**Figure 6B, S3**). For example, M120 forms long chains yet readily
339 forms spores (~100% sporulation frequency). The low sporulation levels of TAL29600 were
340 rather surprising since this strain was isolated from a clinical setting, so it likely forms spores
341 more efficiently in conditions encountered during infection. Notably, when grown on 70:30
342 medium, Clade 5 strains did not appear to form the long chains observed during broth culture
343 and grown on agarose pads. In addition, the spores produced by all *C. difficile* isolates analyzed
344 exhibited similar lengths and proportions despite arising from vegetative cells that varied
345 widely in their cell length (**Figure S4**). Thus, our data suggest that Clade 5 strains alter their cell
346 length and propensity to form chains depending on the media encountered.

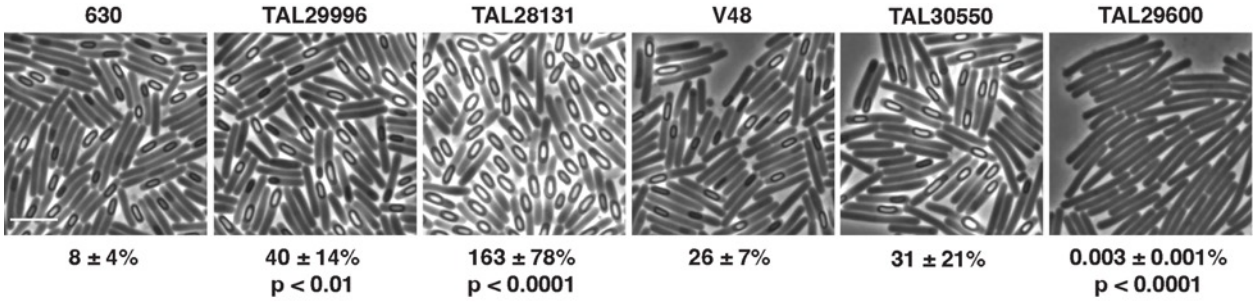

347
348
349 **Figure 6. Sporulation levels in Clade 5 isolates grown on 70:30 medium**. Phase-contrast microscopy
350 of the indicated strains ~24 hrs after sporulation induction. Heat resistance efficiencies, indicated below
351 the respective images, are based on 20-24 hr sporulating cultures and represent the mean and standard
352 deviation for a given strain relative to wild type based on a minimum of three biological replicates.
353 Statistical significance relative to strain 630 was determined using a one-way ANOVA and Tukey's test.
354 The scale bar represents 5 µm.
355
356

357 **Genomic comparisons of Clade 5 strains**

358

359 Since our phenotypic analyses revealed that TAL29996 differs from the 8 additional
360 Clade 5 strains analyzed, we sought to gain insight into the molecular basis for this difference by
361 comparing their genomes. To this end, we sequenced 5 of the Clade 5 strains, including
362 TAL29996, and determined that the average nucleotide identity (ANI) for orthologous genes
363 between the strains ranged from 99.83-99.99% (**Table S1**). Since the pan-genome between the 5
364 strains is 12%, they are quite closely related. A comparison of their pan-genomes revealed that
365 TAL29996 is missing one duplication of *blaR1*, which encodes an integral membrane protein

366 that senses beta-lactams, and a gene region predicted to be involved in nicotinate metabolism
367 compared to the other 4 strains. We also compared the genomes using breseq (44) to identify
368 SNPs that might distinguish TAL29996 from the other strains using strain M120 as the
369 reference, since this strain has been the Clade 5 strain traditionally characterized (30, 45).
370 Around 10 SNPs were unique to TAL29996, but none were clearly implicated in regulating cell
371 separation or peptidoglycan synthesis (**Tables S2, S3**).
372 Since testing whether one or some of these SNPs or absent genes help TAL29996
373 undergo cell separation more efficiently would require genetic manipulation of TAL29996, we
374 instead analyzed the orientation of the *cmr* switch, also known as the Cdi6 DNA invertible
375 element (31, 46). The orientation of the *cmr* switch affects expression of the adjacent *cmrRST*
376 operon, which encodes a non-canonical two-component system, resulting in phase variation of
377 CmrRST. Because CmrRST promotes cell chaining, the orientation of the *cmr* switch determines
378 whether *C. difficile* produces rough or smooth colony morphologies (29, 31, 46). Specifically,
379 cells from rough colonies are highly biased to the ON orientation of the *cmr* switch and exhibit a
380 chaining phenotype, whereas cells from smooth colonies are highly biased to the OFF orientation
381 and do not form chains (31). Consistent with the breseq analyses, manual inspection of the
382 *cmrRST* upstream region revealed that this region is identical between all the Clade 5 strains
383 analyzed (100% identity), including strain TAL29996. In the Illumina whole genome sequencing
384 performed on the subset of 5 Clade 5 strains, the *cmr* switch is in the OFF orientation in the
385 assembled contigs.
386 However, in contrast with the Illumina analyses, qPCR analyses of the *cmr* switch region
387 in the Clade 5 isolates revealed that TAL29996 exhibits a *cmr*-ON frequency of ~20%, whereas
388 the four remaining Clade 5 strains exhibit a *cmr*-ON frequency of between 70-96% on average
389 **(Fig 7**). Furthermore, when we extended these analyses to the four additional Clade 5 strains
390 characterized that also produce chains, we found that they exhibit a *cmr*-ON frequency of
391 between 80-93%. Collectively, these results suggest that the orientation of the *cmr* switch
392 orientation correlates with the propensity to form chains in Clade 5 strains and that most Clade 5
393 strains are biased to the *cmr*-ON orientation even during growth in broth culture.
394 Since the *cmr*-ON state has also been correlated with increased surface motility, we next
395 analyzed the surface motility of Clade 5 strains. After incubation for 5 days, *cmr*-ON strains
396 spread further on agar plates than the TAL29996 *cmr*-OFF strain (**Fig 7B**). Consistent with prior

397 reports, Clade 5 strains whose *cmr* switch is predominantly in the ON orientation exhibited
398 greater and more uniform surface motility. In contrast, TAL29996 exhibited less and more
399 asymmetric surface motility, with fractal-like extensions extending from a couple of sites. The
400 surface motility of TAL29996 resembles the phenotype previously reported for Clade 2 strain
401 R20291, whose *cmr* switch is also predominantly in the OFF position in liquid cultures.
402 However, growth of R20291 on agar medium selects for bacteria with the *cmr* switch in the ON
403 orientation, which leads to asymmetric surface motility on plates (31). These observations
404 suggest that even though TAL29996 is biased to the *cmr*-OFF orientation during broth culture
405 growth, during growth on BHIS agar, a subset of cells switch to the *cmr*-ON orientation, leading
406 to the asymmetric spreading phenotype.
407

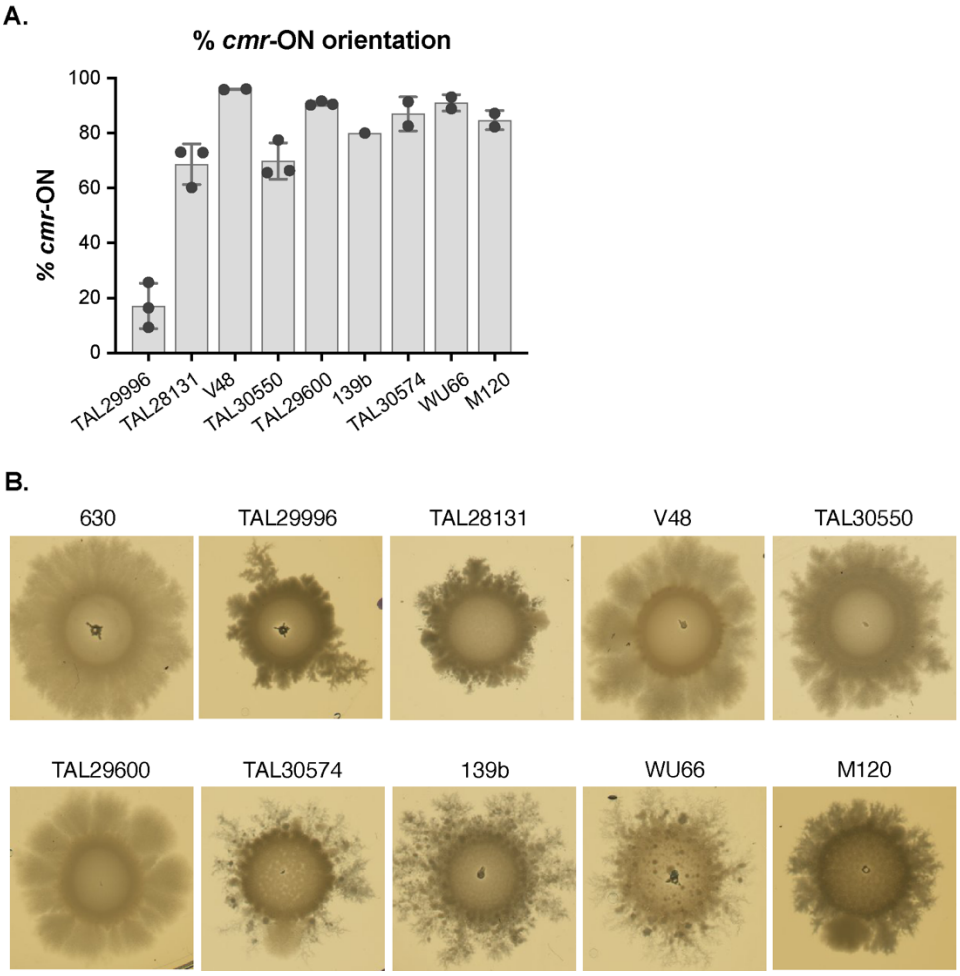

408
409
410 **Figure 7. Orientation of the *cmr* switch correlates with chaining phenotype and surface motility in**
411 **Clade 5 strains.** A. Orientation-specific PCR for detecting the orientation of the *cmr* switch in the

412 indicated strains. B. Representative images of surface motility 5 days after exponentially growing liquid
413 cultures were spotted onto BHIS agar plates.
414
415 Analyses of the surface motility of strains from Clade 1, 2, and 4 revealed that
416 asymmetric motility was more frequently observed in Clade 2 strains. Clade 1 strains exhibited a
417 range of surface motility, from high surface motility with strain 630 to lower surface motility
418 with strain WU38 (**Figure S5**). While analyzing a larger number of Clade 1, 2, and 4 strains
419 would reveal whether there are clade-specific differences in surface motility, the data suggest
420 that Clade 2 strains may exhibit more variability in *cmr* switching within a population during
421 growth on plates, with strain Wup14 exhibiting the least surface motility of the Clade 2 strains
422 tested. Collectively, the data imply that the ON orientation of the *cmr* switch during broth culture
423 growth contributes to the chaining phenotype observed in most Clade 5 strains.
424
425
426 **Discussion**
427
428 While the genetically distinct nature of Clade 5 strains from Clade 1-4 strains is well-
429 established (10, 26), the phenotypic impacts of this genetic diversity are poorly understood,
430 with only one study to our knowledge systematically comparing Clade 5 strains to Clade 1-4
431 strains (10, 26). By phenotypically characterizing *C. difficile* strains from multiple clades using
432 time-lapse microscopy, we discovered that Clade 5 strains have distinct growth properties from
433 the Clade 1, 2, and 4 strains tested. Our analyses of multiple strains from each of Clades 1, 2, 4,
434 and 5 revealed that Clade 5 strains grow more quickly (**Figures 2, 4, S1**) and are more likely to
435 form chains than strains from Clades 1, 2, and 4, irrespective of media type or growth on a
436 surface (**Figures 2, 4, S2**). Notably, these analyses represent the first report of the single-cell
437 growth properties of *C. difficile* to our knowledge and were enabled by our development of a
438 simple method for conducting anaerobic time-lapse microscopy analyses (**Figure 1**) and recent
439 developments in automated image analyses of time-lapse microscopy data (39, 40).
440 Using this time-lapse microscopy method, we discovered that many Clade 5 strains
441 produce extremely long chains of cells (>100 μm in length, **Figures 3, 4**). This chaining
442 phenotype was observed in 8 of 9 Clade 5 strains versus none of the Clade 1, 2, and 4 strains,
443 regardless of whether the cells were grown on agarose pads or in broth culture. Thus, Clade 5
444 strains appear to undergo cell separation less frequently than strains from other Clades. The

445 exception to this conclusion is Clade 5 strain TAL29996, which did not form chains but
446 nevertheless grew at similarly fast rates as the other Clade 5 strains (**Figure 4**). Taken together,
447 these data suggest that faster growth is likely a characteristic that distinguishes Clade 5 strains
448 from Clade 1, 2, and 4 strains.

449 Our genomic analyses suggest that a driving factor of the chaining phenotype of Clade 5
450 strains is their propensity to have the *cmr* switch in the ON orientation (**Figure 7**), which
451 increases the expression of an operon encoding a signal transduction system that induces
452 chaining (31). This conclusion is based on our finding that the non-chaining TAL29996 strain
453 exhibits a *cmr*-ON orientation frequency of 20%, whereas the 8 additional Clade 5 strains tested
454 exhibited *cmr*-ON orientation frequencies of between ~70-95% (**Figure 7**). In addition, strain
455 TAL29996 exhibited less surface motility during growth on agar plates, with only a fraction of
456 the population spreading on the surface relative to the more uniform spreading observed for the
457 other 8 Clade 5 strains (**Figure 7**).

458 Previous work in Clade 2 strain R20291 has shown that growth on agar plates promotes
459 selection of *cmr*-ON bacteria, and increased c-di-GMP during surface growth may also promote
460 *cmrRST* expression (29), so Clade 5 strain TAL29996 may exhibit a similar surface-inducible
461 expression of the *cmrRST* operon. Indeed, the chaining phenotype of Clade 5 strains was more
462 frequent and extensive during time-lapse microscopy analyses on agarose pads compared to
463 broth culture-grown cells (**Figures 4, 5**). Thus, the chaining phenotype of Clade 5 strains may
464 be similarly responsive to c-di-GMP levels during growth on a surface (29). While testing this
465 hypothesis will depend on the ability to genetically manipulate Clade 5 strains, it is tempting to
466 speculate that *cmrRST* expression is an important determinant of the growth properties of Clade
467 5 strains. Expression of this operon in Clade 2 strain R20291 not only promotes chaining and
468 surface motility in a Type IV pilus-independent manner, it also negatively regulates biofilm
469 formation and flagellar motility (31). In addition, growth conditions favoring flagellar motility
470 select against *cmr*-ON bacteria. Since Clade 5 strains lack flagellar motility (12), they may be
471 "primed" to exhibit surface motility in the absence of selection against the *cmr*-ON state.
472 Regardless, analyzing the regulation of c-di-GMP in different growth conditions in Clade 5
473 strains, particularly for TAL29996 relative to the other strains, will likely provide insight into
474 the mechanisms that drive the higher incidence of *cmr*-ON cells in most Clade 5 strains.

475 Even though Clade 5 strains form long chains and produce longer cells than strains from
476 the other clades, neither cell nor chain length was predictive of the propensity to sporulate
477 (**Figure 6**). Clade 5 strains exhibited wildly different sporulation frequencies, with TAL29600
478 forming spores inefficiently (~5,000-fold less efficiently than most Clade 5 strains). While little
479 is known about the mechanisms regulating sporulation initiation outside of strains 630 and
480 R20291, future analyses of strain TAL29600, which sporulates poorly under the laboratory
481 media tested (**Figure 6**), could provide insight into the molecular determinants of sporulation in
482 Clade 5 strains. For example, differences in gene presence or polymorphisms in several c-di-
483 GMP-related genes were observed in TAL29600 relative to the other Clade 5 strains (**Table**
484 **S2**), and c-di-GMP has also been implicated in regulating sporulation initiation events through
485 an unknown mechanism (47, 48). Thus, analyzing the contribution of these genes in future work
486 could provide important insight into c-di-GMP-mediated regulation of sporulation.
487 The variable sporulation levels observed for the nine Clade 5 strains analyzed in this
488 manuscript contrast with the findings of a previous study, which reported that Clade 5 strains
489 sporulate at lower rates in the presence of glucose and fructose (26). Kumar *et al*. previously
490 correlated phenotypic differences in sporulation and mouse colonization between Clade 5
491 strains vs. Clade 1-4 strains to their finding that genes involved in sporulation and the
492 metabolism of simple sugars are under positive selection in Clade 1-4 strains (26). However, the
493 five Clade 5 strains analyzed by Kumar *et al*. all exhibited very low sporulation frequencies
494 under the conditions tested. While we used different conditions to induce sporulation in the
495 present study than those by Kumar *et al*., our analyses of nine Clade 5 strains indicate that there
496 are marked phenotypic differences in sporulation frequency within this clade. Thus, analyzing
497 more strains within a clade may reveal fewer differences between clades. A caveat to our
498 analyses is that *C. difficile* strains exhibit considerable genetic diversity even within a ribotype
499 (20, 22), so our conclusions may only reflect the behavior of RT078 Clade 5 strains. It is also
500 possible that analyzing more strains within this ribotype will reveal a broader spectrum of
501 phenotypes than the somewhat bimodal ones we have reported with respect to cell length and
502 chaining propensity (**Figures 2, 3**). Indeed, a recent analysis of a large number of RT027 strains
503 indicates that strains within this ribotype can exhibit marked differences in virulence in mice
504 (22) despite these strains traditionally being associated with "epidemic" outbreaks in hospital
505 setting.

While addressing these questions will depend on analyzing a larger number of strains from each clade, an important outcome of our study is its development of a facile method for conducting time-lapse microscopy under anaerobic conditions. Although this method is a closed system, i.e. no additional reagents can be introduced once the bacteria are inoculated onto the pad in the anaerobic chamber, it could be coupled to recently developed anaerobic imaging tags based on fluorogen-activated proteins (49). Thus, there are many potential applications for this simple method for studying the growth of anaerobes over time at the single-cell level.

Materials and Methods

Bacterial strains and growth conditions

All *C. difficile* strains were grown on brain heart infusion (BHIS) medium supplemented with 0.5% w/v yeast extract and 0.1% w/v L-cysteine with taurocholate (TCA; 0.1% w/v; 1.9 mM). Strains were sub-cultured into tryptone yeast extract (TY) broth supplemented with 0.1% w/v L-cysteine (TYC medium) prior to inoculation onto the time-lapse microscopy agarose pads. All strains were grown at 37°C under anaerobic conditions using a gas mixture of 85% hydrogen, 5% CO2, and 10% H2. For time-lapse experiments, 1.5% agarose pads were used supplemented with TYC medium as described above. Sporulation analyses were carried out on 70:30 medium (70% BHIS and 30% SMC) for 24h as described previously (50).

Anaerobic time-lapse imaging of C. difficile growth

All imaging was carried out on a Leica DMi8 inverted microscope with a HC plan apochromat 63x 1.4 NA oil immersion phase contrast objective. Fluorescent membrane staining experiments were done with a Lumencor Spectra X light source, coupled with an XLED-QP quadruple-band dichroic beam-splitter (Leica) (transmission: 415, 470, 570, and 660 nm) along with an external emission filter wheel (Leica). FM4-64 was excited using a 470nm LED through a 470/20nm excitation filter and emitted light was filtered through 590/50nm emission filter and captured with a Leica DFC9000GTC sCMOS camera. All experiments were carried out at 37°C using a microscope incubation system (Pecon), Leica Adaptive Focus Control hardware autofocus, and a high precision stage (Pecon) were used for all imaging experiments.

For time-lapse imaging of *C. difficile* growth all bacterial strains were grown in 2 mL liquid TY medium to a turbid OD600 > 2-3; after 2 hours of growth, bacteria were diluted 1:100 for Clade 5 strains and all other strains were diluted 1:50 in fresh media and grown to mid-log stage (OD600 0.4-0.7).

An imaging chamber with a gas-tight seal was constructed using a 125 µL Gene Frame (Thermo Fisher) adhered to a glass slide generating a well for growth medium. The slide was then transferred to the anaerobic chamber. In the anaerobic chamber, the gene frame was filled with 500µl 1.5% Top vision low melting point agarose and tryptone yeast extract media containing 0.1% w/v L-cysteine to scavenge oxygen and maintain anaerobic conditions. While the agarose was molten, a second clean slide was placed over the top and the agar pad was placed on a frozen small freezer block (for holding PCR strip tubes) for 10-30 minutes until the agarose-media mixture was solid. For experiments where FM4-64 was used, agarose pads were

549 made the same way, with the addition of FM4-64 to a final concentration of 1 μg/mL directly to
550 the agarose/media solution prior to making the agar pad.
551 The agar pad was dried for 5-10 minutes until visible liquid on the surface of the pad
552 was evaporated. 1 μL of mid-log cells were spotted on the pad, dried, and a #1.5 coverslip
553 (VWR) was adhered to the Gene Frame. The cells were imaged at 37°C until they reached
554 confluency in the field of view. This was anywhere from 2.5 hours for Clade 5 strains to 6 hours
555 for Clades 1-4 for all experiments with images taken at 5-minute intervals.
556
557 *Image analysis, computing hardware, and statistical analysis.*
558 All movie frames were trimmed to the point when cells were not overlapping and out of
559 focus regions were cropped. The resulting images were analyzed using the Python library
560 DeLTA 2.0 (39, 40). All image and data analyses were done on a PC running
561 Windows 10 equipped with an AMD Ryzen 5900HX 8-core CPU, 32GB DDR4 RAM, 2 1TB
562 NVME SSDs, and an NVIDIA RTX3080 GPU with 16GB VRAM. Analysis of the output data
563 and data visualizations were done in Python using Matplotlib/Seaborn,
564 Pandas, Numpy, Scipy, and the Statannotations library.
565
566 **Septum detection**
567 The image processing starts with the masks generated using DeLTA 2.0. First, we performed
568 erosion on the mask with a disk of radius of 1 pixel to avoid effects of the membrane fluorescence.
569 The photo was cropped following the eroded mask contour. Hence, only the interior of the contour
570 was considered. Pixel values were rescaled such as the minimum pixel value of inner pixels was
571 mapped to 0 and the maximum is mapped to 255. We set a threshold intensity as the pixel value
572 of the 95% quantile of pixel intensities. The image was slightly blurred by convolution with a
573 Gaussian filter with standard deviation of 2 pixels. The septum corresponds to the contours found
574 after performing an adaptive thresholding based on thresholds defined using a Gaussian-weighted
575 method. This thresholding was performed using the open cv2 library in Python. The resultant
576 contours were manually verified from videos generated using the tracking from the outputs from
577 DeLTA. The manual validation mainly involved filling in the time points where the algorithm
578 missed a ring that was visible in the video. We did not assume the existence of a ring if the
579 algorithm did not detect it in a previous ,m,frame.
580
581 **Cell length estimation**
582 We measured the cell projected area from the DeLTA contours of the images as the pixel amount
583 of the contours. However, estimating the cell length was challenging because some cells were very
584 long and bent. To overcome this problem, we selected 30 images of three different cells (from
585 strains 630, TAL3050 and TAL28131) that were straight and had different lengths. For these cells,
586 we calculated the cell length as the longest side of the minimum bounding rectangle of the contour.
587 From these lengths of straight cells, we also estimated the best cell width as the average of the
588 projected area divided by the length. Considering the extreme cell length, the effects of the rounded
589 tips were negligible and the rectangle shape adequately approximated length. We verifed that this
590 mean value showed low variability for the three strains. Then, we used this width value to estimate
591 the length of all the cells, including the bent ones, by dividing their projected area by the width.
592 This way, we obtained a consistent measure of cell length that was independent of bending.
593
594 **Elongation rate estimation**

595 We tracked the cell size over time and identified the division points as the ones where the cell size
596 (projected area) dropped by more than 30% compared to the current cell size value. We fitted an
597 exponential function (with base e) of time to the data points between two divisions and estimated
598 the elongation rate from the exponent of the best fit. We expressed the elongation rate in
599 doublings/hr, which means how many times the cell size doubles in one hour. For example, an
600 elongation rate of 2 doubling/hr means that the cell size doubles two times in 1 hr, which
601 corresponds to an exponent of 2ln(2) 1/hr. For the statistics, we only included the elongation rates
602 that had a high quality of fit, with an R2 coefficient greater than 0.9.
603
604 **Bulk growth measurements**. Starter cultures were grown until early stationary phase in BHIS
605 (or TYC medium as indicated) then back-diluted 1:50 into BHIS (or TYC medium). When the
606 cultures reached an OD_{600} of 0.5, they were back-diluted 1:25 into 200 µL of either BHIS or
607 TYC in a flat 96 well polystyrene plate (CellTreat). The OD_{600} was analyzed every 15 min for 24
608 hrs in a BioTek Epoch plate reader with shaking. Bulk growth measurements are based on a
609 minimum of three independent replicates across a minimum of 2 experiments.
610
611 **Sporulation assays**. Starter cultures were grown until early stationary phase in BHIS then back-
612 diluted 1:50 into BHIS. When the cultures reached an OD_{600} between 0.35 and 0.75, 120 µL of
613 the culture was spread onto 70:30 (70% SMC media and 30% BHIS media) agar plates (40 ml
614 media per plate) and then incubated for 20-24 hrs before the sporulating cells were scraped from
615 the plate into phosphate-buffered saline (PBS). Sporulation levels were visualized by phase-
616 contrast microscopy as previously described (51).
617
618 **Heat resistance assay**. Heat-resistant spore formation was measured 20-24 hrs after sporulation
619 was induced on 70:30 agar plates as previously described (50). The percent sporulation of given
620 culture represents the ratio of heat-resistant colony-forming units (CFUs) to total CFUs. Percent
621 sporulation was determined from a minimum of 3 biological replicates.
622
623 **Spore purification**. Spores were purified as previously described (52) by scraping up
624 sporulating cells incubated on 70:30 medium for 3 days into ice-cold H_2O. The cells were
625 washed several times in ice-water over the course of a day and incubated on ice overnight. The
626 following morning, the sample was pelleted, and cells were resuspended in 1 X DNAse buffer
627 (New England Biolabs) and then treated with DNAse (New England Biolabs) for 30 min at 37˚C.
628 The samples was washed one more time before being resuspended in 20% Histodenz and then
629 layered onto a 50% Histodenz layer. The resulting mixture was pelleted and the supernatant was
630 aspirated off using a vacuum aspirator. The pelleted spores were washed in ice-cold water 2-3
631 times and the optical density of the purified spores was measured.
632
633 **Genomic DNA preparation**. Starter cultures were grown until early stationary phase in BHIS
634 then back-diluted 1:50 into BHIS and grown until an OD_{600} of around 0.7-0.8 was reached. 10
635 mL of the culture was pelleted and then frozen at -80˚C. After thawing the sample, it was
636 resuspended in a 25% sucrose TE buffer (10 mM Tris, 1mM EDTA), incubated with 100 mg/mL
637 lysozyme for 37˚C for 1 hr. After the cultures tarted to lyse, proteinase K, RNAse A, EDTA,
638 Sarkosyl, and NaCl was added. Phenol:Chloroform:IAA (25:24:1) was added to extract proteins,
639 gently mixed, and then the sample was pelleted to separate the phenol and aqueous layer. The
640 aqueous layer was then added to Chloroform:IAA (24:1), mixed gently, then centrifuged. The
641 aqueous layer was then precipitated using isopropanol and incubated at -20˚C for a minimum of

642 15 min. The precipitated DNA was pelleted and then washed with 70% ethanol. The pellet was
643 air dried and then gently resuspended in 10 mM Tris pH 8.0 elution buffer.
644
645 **Genomic analyses**. Genomic DNA was sequenced by MiGS at the University of Pittsburgh
646 (now SeqCenter) according to their standard protocol. Libraries were sequenced on an Illumina
647 NextSeq 500 platform to generate paired-end 150 bp reads. Illumina reads of RT078 genomes
648 were assembled into contigs using SPAdes (v3.13.0),(53) and genes were called and annotated
649 using Prokka (v1.11).(54) Assembled and annotated contigs of five RT078 strains (TAL28131,
650 TAL29600, TAL29996, TAL30550, TAL30574) were applied for pangenomic analysis. Default
651 settings were used based on the Anvi'o workflow for microbial pangenomcis with adjustments
652 for minbit as 0.5 and mcl-inflation as 10.(55-57) For SNPs analyses, reads of five RT078
653 genomes were aligned to the reference M120 and variants were called by breseq (v. 0.38.1) by
654 default settings.(58)
655
656 **qPCR analyses**. Each genomic DNA sample was analyzed by qPCR with primers that amplify
657 the *cmr*-ON sequence orientation, the *cmr*-OFF orientation, or the reference gene *rpoA* (31) .
658 Each 20-µL qPCR reaction consisted of 100 ng genomic DNA, 100 nM primers, and SensiMix™
659 SYBR® reagents (Bioline). The reactions were run on a LightCycler® 96 (Roche Diagnostics),
660 and *cmr* switch orientation frequencies were calculated as described previously (29).
661
662 **Surface motility assays**
663 Starter cultures were grown until early stationary phase in BHIS then back-diluted 1:50 into
664 BHIS and grown until an OD_{600} of 0.5 was reached. 10 µL of the exponential-phase cultures
665 were then spotted onto BHIS plates and incubated at 37˚C for 5 days after which the plates were
666 scanned using a flatbed scanner.
667
668 *Author contribution statement*
669 J.W.R. conducted all live-cell microscopy experiments and analyzed the single-cell data.
670 C.A.N.A. generated data visualizations from the time-lapse microscopy data, developed the
671 method for identifying septa within chains that had not initiated cell separation, and calculated
672 elongation rates and cell lengths. I.N. and A.S. conducted sporulation analyses and liquid
673 culture experiments. J.W.R., R.T., and A.S conceptualized all experiments with input from .
674 Q.D. and A.S extracted genomic DNA and visualized cells at different growth phases. Q.D.
675 conducted all the genomic analyses and genome comparisons. N.D. and I.N. conducted spore
676 purification analyses and imaging. B.A. and IE developed and optimized methods for
677 constructing agarose pads that could support anaerobic growth in an ambient atmosphere.
678 M.J.D. developed the DeLTA 2.0 analysis pipeline. A.M. conducted qPCRs to determine *cmr*
679 switch orientation in Clade 5 isolates. Writing was by J.W.R and A.S with input from all the
680 authors.
681
682
683 **Table 1. *Clostridioides difficile* clinical isolates used in this study**
684

Strain Name	Clade	Ribotype	ST group	Source	Reference
630	1	012	2	Zurich, 1982 (Sanger Institute)	(59)
R20291	2	027	1	London, 2006 (Sanger Institute)	(60)

M68	4	017	81	Dublin, 2006 (Sanger Institute)	(45)
M120	5	078	11	UK, 2007 (Sanger Institute)	(45)
TAL28131	5	078	11	Tufts Medical Center	This paper
TAL29600	5	078	11	Tufts Medical Center	This paper
TAL29996	5	078	11	Tufts Medical Center	This paper
TAL30550	5	078	11	Tufts Medical Center	This paper
TAL30574	5	078	11	Tufts Medical Center	This paper
V48	5	078	11	Brigham & Women's Hospital	This paper
139b	5	078	11	Memorial Sloan Kettering	(20)
WU66	5	078	11	Barnes-Jewish Hospital	(20)
BBL2	1	012	2	Memorial Sloan Kettering	(20)
WU38	1	012	2	Barnes-Jewish Hospital	(20)
190B	1	087	46	Memorial Sloan Kettering	(20)
Wup14	2	027	1	Barnes-Jewish Hospital	(20)
BBL4	2	027	1	Memorial Sloan Kettering	(20)
186A	2	027	1	Memorial Sloan Kettering	(20)

Memorial Sloan Kettering Cancer Center (MSK), Barnes-Jewish Hospital (BJH)

References

1. Desai K, Gupta SB, Dubberke ER, Prabhu VS, Browne C, Mast TC. 2016. Epidemiological and economic burden of Clostridium difficile in the United States: estimates from a modeling approach. BMC Infect Dis 16:303.
2. Guh AY, Mu Y, Winston LG, Johnston H, Olson D, Farley MM, Wilson LE, Holzbauer SM, Phipps EC, Dumyati GK, Beldavs ZG, Kainer MA, Karlsson M, Gerding DN, McDonald LC, Emerging Infections Program Clostridioides difficile Infection Working G. 2020. Trends in U.S. Burden of Clostridioides difficile Infection and Outcomes. N Engl J Med 382:1320-1330.
3. Shen A. 2020. Clostridioides difficile Spore Formation and Germination: New Insights and Opportunities for Intervention. Annu Rev Microbiol 74:545-566.
4. Abt MC, McKenney PT, Pamer EG. 2016. Clostridium difficile colitis: pathogenesis and host defence. Nat Rev Microbiol doi:10.1038/nrmicro.2016.108.
5. Theriot CM, Young VB. 2015. Interactions Between the Gastrointestinal Microbiome and Clostridium difficile. Annu Rev Microbiol 69:445-61.
6. Kordus SL, Thomas AK, Lacy DB. 2022. Clostridioides difficile toxins: mechanisms of action and antitoxin therapeutics. Nat Rev Microbiol 20:285-298.
7. Maroo S, Lamont J. 2006. Recurrent Clostridium difficile. Gastroenterology 130:1311-1316.
8. Zanella Terrier MC, Simonet ML, Bichard P, Frossard JL. 2014. Recurrent Clostridium difficile infections: the importance of the intestinal microbiota. World J Gastroenterol 20:7416-23.
9. Knight DR, Elliott B, Chang BJ, Perkins TT, Riley TV. 2015. Diversity and Evolution in the Genome of Clostridium difficile. Clin Microbiol Rev 28:721-41.

713 10. Knight DR, Imwattana K, Kullin B, Guerrero-Araya E, Paredes-Sabja D, Didelot X,
714 Dingle KE, Eyre DW, Rodriguez C, Riley TV. 2021. Major genetic discontinuity and
715 novel toxigenic species in Clostridioides difficile taxonomy. Elife 10.
716 11. Norsigian CJ, Danhof HA, Brand CK, Midani FS, Broddrick JT, Savidge TC, Britton
717 RA, Palsson BO, Spinler JK, Monk JM. 2022. Systems biology approach to functionally
718 assess the Clostridioides difficile pangenome reveals genetic diversity with
719 discriminatory power. Proc Natl Acad Sci U S A 119:e2119396119.
720 12. Knight DR, Kullin B, Androga GO, Barbut F, Eckert C, Johnson S, Spigaglia P, Tateda
721 K, Tsai PJ, Riley TV. 2019. Evolutionary and Genomic Insights into Clostridioides
722 difficile Sequence Type 11: a Diverse Zoonotic and Antimicrobial-Resistant Lineage of
723 Global One Health Importance. mBio 10.
724 13. Seth-Smith HMB, Biggel M, Roloff T, Hinic V, Bodmer T, Risch M, Casanova C,
725 Widmer A, Sommerstein R, Marschall J, Tschudin-Sutter S, Egli A. 2021. Transition
726 From PCR-Ribotyping to Whole Genome Sequencing Based Typing of Clostridioides
727 difficile. Front Cell Infect Microbiol 11:681518.
728 14. Jain C, Rodriguez RL, Phillippy AM, Konstantinidis KT, Aluru S. 2018. High throughput
729 ANI analysis of 90K prokaryotic genomes reveals clear species boundaries. Nat Commun
730 9:5114.
731 15. Dingle KE, Elliott B, Robinson E, Griffiths D, Eyre DW, Stoesser N, Vaughan A,
732 Golubchik T, Fawley WN, Wilcox MH, Peto TE, Walker AS, Riley TV, Crook DW,
733 Didelot X. 2014. Evolutionary history of the Clostridium difficile pathogenicity locus.
734 Genome Biol Evol 6:36-52.
735 16. Mengoli M, Barone M, Fabbrini M, D'Amico F, Brigidi P, Turroni S. 2022. Make It Less
736 difficile: Understanding Genetic Evolution and Global Spread of Clostridioides difficile.
737 Genes (Basel) 13.
738 17. Endres BT, Begum K, Sun H, Walk ST, Memariani A, Lancaster C, Gonzales-Luna AJ,
739 Dotson KM, Basseres E, Offiong C, Tupy S, Kuper K, Septimus E, Arafat R, Alam MJ,
740 Zhao Z, Hurdle JG, Savidge TC, Garey KW. 2019. Epidemic Clostridioides difficile
741 Ribotype 027 Lineages: Comparisons of Texas Versus Worldwide Strains. Open Forum
742 Infect Dis 6:ofz013.
743 18. McDonald LC, Killgore GE, Thompson A, Owens RC, Jr., Kazakova SV, Sambol SP,
744 Johnson S, Gerding DN. 2005. An epidemic, toxin gene-variant strain of Clostridium
745 difficile. N Engl J Med 353:2433-41.
746 19. Clements AC, Magalhaes RJ, Tatem AJ, Paterson DL, Riley TV. 2010. Clostridium
747 difficile PCR ribotype 027: assessing the risks of further worldwide spread. Lancet Infect
748 Dis 10:395-404.
749 20. Lewis BB, Carter RA, Ling L, Leiner I, Taur Y, Kamboj M, Dubberke ER, Xavier J,
750 Pamer EG. 2017. Pathogenicity Locus, Core Genome, and Accessory Gene Contributions
751 to Clostridium difficile Virulence. mBio 8.
752 21. Merrigan M, Venugopal A, Mallozzi M, Roxas B, Viswanathan VK, Johnson S, Gerding
753 DN, Vedantam G. 2010. Human hypervirulent Clostridium difficile strains exhibit
754 increased sporulation as well as robust toxin production. J Bacteriol 192:4904-11.
755 22. Dong Q, Lin H, Allen MM, Garneau JR, Sia JK, Smith RC, Haro F, McMillen T, Pope
756 RL, Metcalfe C, Burgo V, Woodson C, Dylla N, Kohout C, Sundararajan A, Snitkin ES,
757 Young VB, Fortier LC, Kamboj M, Pamer EG. 2023. Virulence and genomic diversity

758 among clinical isolates of ST1 (BI/NAP1/027) Clostridioides difficile. Cell Rep
759 42:112861.
760 23. Shaw HA, Preston MD, Vendrik KEW, Cairns MD, Browne HP, Stabler RA, Crobach
761 MJT, Corver J, Pituch H, Ingebretsen A, Pirmohamed M, Faulds-Pain A, Valiente E,
762 Lawley TD, Fairweather NF, Kuijper EJ, Wren BW. 2020. The recent emergence of a
763 highly related virulent Clostridium difficile clade with unique characteristics. Clin
764 Microbiol Infect 26:492-498.
765 24. Li C, Harmanus C, Zhu D, Meng X, Wang S, Duan J, Liu S, Fu C, Zhou P, Liu R, Wu A,
766 Kuijper EJ, Smits WK, Fu L, Sun X. 2018. Characterization of the virulence of a non-
767 RT027, non-RT078 and binary toxin-positive Clostridium difficile strain associated with
768 severe diarrhea. Emerg Microbes Infect 7:211.
769 25. Imwattana K, Rodriguez C, Riley TV, Knight DR. 2021. A species-wide genetic atlas of
770 antimicrobial resistance in Clostridioides difficile. Microb Genom 7.
771 26. Kumar N, Browne HP, Viciani E, Forster SC, Clare S, Harcourt K, Stares MD, Dougan
772 G, Fairley DJ, Roberts P, Pirmohamed M, Clokie MRJ, Jensen MBF, Hargreaves KR, Ip
773 M, Wieler LH, Seyboldt C, Noren T, Riley TV, Kuijper EJ, Wren BW, Lawley TD. 2019.
774 Adaptation of host transmission cycle during Clostridium difficile speciation. Nat Genet
775 51:1315-1320.
776 27. Knetsch CW, Kumar N, Forster SC, Connor TR, Browne HP, Harmanus C, Sanders IM,
777 Harris SR, Turner L, Morris T, Perry M, Miyajima F, Roberts P, Pirmohamed M, Songer
778 JG, Weese JS, Indra A, Corver J, Rupnik M, Wren BW, Riley TV, Kuijper EJ, Lawley
779 TD. 2018. Zoonotic Transfer of Clostridium difficile Harboring Antimicrobial Resistance
780 between Farm Animals and Humans. J Clin Microbiol 56.
781 28. Lim SC, Knight DR, Riley TV. 2020. Clostridium difficile and One Health. Clin
782 Microbiol Infect 26:857-863.
783 29. Garrett EM, Mehra A, Sekulovic O, Tamayo R. 2021. Multiple Regulatory Mechanisms
784 Control the Production of CmrRST, an Atypical Signal Transduction System in
785 Clostridioides difficile. mBio 13:e0296921.
786 30. Thanissery R, Winston JA, Theriot CM. 2017. Inhibition of spore germination, growth,
787 and toxin activity of clinically relevant C. difficile strains by gut microbiota derived
788 secondary bile acids. Anaerobe 45:86-100.
789 31. Garrett EM, Sekulovic O, Wetzel D, Jones JB, Edwards AN, Vargas-Cuebas G, McBride
790 SM, Tamayo R. 2019. Phase variation of a signal transduction system controls
791 Clostridioides difficile colony morphology, motility, and virulence. PLoS Biol
792 17:e3000379.
793 32. Ackermann M. 2015. A functional perspective on phenotypic heterogeneity in
794 microorganisms. Nat Rev Microbiol 13:497-508.
795 33. Aldridge BB, Fernandez-Suarez M, Heller D, Ambravaneswaran V, Irimia D, Toner M,
796 Fortune SM. 2012. Asymmetry and aging of mycobacterial cells lead to variable growth
797 and antibiotic susceptibility. Science 335:100-4.
798 34. Anjuwon-Foster BR, Tamayo R. 2017. A genetic switch controls the production of
799 flagella and toxins in Clostridium difficile. PLoS Genet 13:e1006701.
800 35. Anjuwon-Foster BR, Tamayo R. 2018. Phase variation of Clostridium difficile virulence
801 factors. Gut Microbes 9:76-83.

802 36. Kint N, Janoir C, Monot M, Hoys S, Soutourina O, Dupuy B, Martin-Verstraete I. 2017.
803 The alternative sigma factor sigma(B) plays a crucial role in adaptive strategies of
804 Clostridium difficile during gut infection. Environ Microbiol 19:1933-1958.
805 37. Courson DS, Pokhrel A, Scott C, Madrill M, Rinehold AJ, Tamayo R, Cheney RE,
806 Purcell EB. 2019. Single cell analysis of nutrient regulation of Clostridioides
807 (Clostridium) difficile motility. Anaerobe 59:205-211.
808 38. de Jong IG, Beilharz K, Kuipers OP, Veening JW. 2011. Live Cell Imaging of Bacillus
809 subtilis and Streptococcus pneumoniae using Automated Time-lapse Microscopy. J Vis
810 Exp doi:10.3791/3145.
811 39. Lugagne JB, Lin H, Dunlop MJ. 2020. DeLTA: Automated cell segmentation, tracking,
812 and lineage reconstruction using deep learning. PLoS Comput Biol 16:e1007673.
813 40. O'Connor OM, Alnahhas RN, Lugagne JB, Dunlop MJ. 2022. DeLTA 2.0: A deep
814 learning pipeline for quantifying single-cell spatial and temporal dynamics. PLoS
815 Comput Biol 18:e1009797.
816 41. Sauls JT, Cox SE, Do Q, Castillo V, Ghulam-Jelani Z, Jun S. 2019. Control of Bacillus
817 subtilis Replication Initiation during Physiological Transitions and Perturbations. mBio
818 10.
819 42. Narula J, Kuchina A, Zhang F, Fujita M, Suel GM, Igoshin OA. 2016. Slowdown of
820 growth controls cellular differentiation. Mol Syst Biol 12:871.
821 43. Eswaramoorthy P, Duan D, Dinh J, Dravis A, Devi SN, Fujita M. 2010. The threshold
822 level of the sensor histidine kinase KinA governs entry into sporulation in Bacillus
823 subtilis. J Bacteriol 192:3870-82.
824 44. Deatherage DE, Traverse CC, Wolf LN, Barrick JE. 2014. Detecting rare structural
825 variation in evolving microbial populations from new sequence junctions using breseq.
826 Front Genet 5:468.
827 45. He M, Sebaihia M, Lawley T, Stabler R, Dawson L, Martin M, Holt K, Seth-Smith H,
828 Quail M, Rance R, Brooks K, Churcher C, Harris D, Bentley S, Burrows C, Clark L,
829 Corton C, Murray V, Rose G, Thurston S, van Tonder A, Walker D, Wren B, Dougan G,
830 Parkhill J. 2010. Evolutionary dynamics of Clostridium difficile over short and long time
831 scales. Proceedings of the National Academy of Sciences of the United States of America
832 107:7527-7532.
833 46. Sekulovic O, Mathias Garrett E, Bourgeois J, Tamayo R, Shen A, Camilli A. 2018.
834 Genome-wide detection of conservative site-specific recombination in bacteria. PLoS
835 Genet 14:e1007332.
836 47. Dhungel BA, Govind R. 2021. Phase-variable expression of pdcB, a phosphodiesterase,
837 influences sporulation in Clostridioides difficile. Mol Microbiol 116:1347-1360.
838 48. Edwards AN, Willams CL, Pareek N, McBride SM, Tamayo R. 2021. c-di-GMP Inhibits
839 Early Sporulation in Clostridioides difficile. mSphere 6:e0091921.
840 49. Streett H, Charubin K, Papoutsakis ET. 2021. Anaerobic fluorescent reporters for cell
841 identification, microbial cell biology and high-throughput screening of microbiota and
842 genomic libraries. Curr Opin Biotechnol 71:151-163.
843 50. Shen A, Fimlaid KA, Pishdadian K. 2016. Inducing and Quantifying Clostridium difficile
844 Spore Formation. Methods Mol Biol 1476:129-42.
845 51. Pishdadian K, Fimlaid KA, Shen A. 2015. SpoIIID-mediated regulation of sigma(K)
846 function during Clostridium difficile sporulation. Mol Microbiol 95:189-208.

847 52. Fimlaid KA, Jensen O, Donnelly ML, Francis MB, Sorg JA, Shen A. 2015. Identification
848 of a Novel Lipoprotein Regulator of Clostridium difficile Spore Germination. PLoS
849 Pathogens doi:10.1371/journal.ppat.1005239.
850 53. Prjibelski A, Antipov D, Meleshko D, Lapidus A, Korobeynikov A. 2020. Using SPAdes
851 De Novo Assembler. Curr Protoc Bioinformatics 70:e102.
852 54. Seemann T. 2014. Prokka: rapid prokaryotic genome annotation. Bioinformatics
853 30:2068-9.
854 55. Benedict MN, Henriksen JR, Metcalf WW, Whitaker RJ, Price ND. 2014. ITEP: an
855 integrated toolkit for exploration of microbial pan-genomes. BMC Genomics 15:8.
856 56. Eren AM, Kiefl E, Shaiber A, Veseli I, Miller SE, Schechter MS, Fink I, Pan JN, Yousef
857 M, Fogarty EC, Trigodet F, Watson AR, Esen OC, Moore RM, Clayssen Q, Lee MD,
858 Kivenson V, Graham ED, Merrill BD, Karkman A, Blankenberg D, Eppley JM, Sjodin
859 A, Scott JJ, Vazquez-Campos X, McKay LJ, McDaniel EA, Stevens SLR, Anderson RE,
860 Fuessel J, Fernandez-Guerra A, Maignien L, Delmont TO, Willis AD. 2021. Community-
861 led, integrated, reproducible multi-omics with anvi'o. Nat Microbiol 6:3-6.
862 57. van Dongen S, Abreu-Goodger C. 2012. Using MCL to extract clusters from networks.
863 Methods Mol Biol 804:281-95.
864 58. Deatherage DE, Barrick JE. 2014. Identification of mutations in laboratory-evolved
865 microbes from next-generation sequencing data using breseq. Methods Mol Biol
866 1151:165-88.
867 59. Sebaihia M, Wren B, Mullany P, Fairweather N, Minton N, Stabler R, Thomson N,
868 Roberts A, Cerdeño-Târraga A, Wang H, Holden M, Wright A, Churcher C, Quail M,
869 Baker S, Bason N, Brooks K, Chillingworth T, Cronin A, Davis P, Dowd L, Fraser A,
870 Feltwell T, Hance Z, Holroyd S, Jagels K, Moule S, Mungall K, Price C, Rabbinowitsch
871 E, Sharp S, Simmonds M, Stevens K, Unwin L, Whithead S, Dupuy B, Dougan G,
872 Barrell B, Parkhill J. 2006. The multidrug-resistant human pathogen Clostridium difficile
873 has a highly mobile, mosaic genome. Nature genetics 38:779-786.
874 60. Stabler R, He M, Dawson L, Martin M, Valiente E, Corton C, Lawley T, Sebaihia M,
875 Quail M, Rose G, Gerding D, Gibert M, Popoff M, Parkhill J, Dougan G, Wren B. 2009.
876 Comparative genome and phenotypic analysis of Clostridium difficile 027 strains
877 provides insight into the evolution of a hypervirulent bacterium. Genome biology 10.
878